Radiative effects driven by shock waves in cavity-less four-wave mixing combs

Matteo Conforti, Stefano Trillo

Radiative effects driven by shock waves in cavity-less four-wave mixing combs

Matteo Conforti [1] **and Stefano Trillo** [2]

[1] *PhLAM/IRCICA, CNRS-Université Lille 1, UMR 8523/USR 3380, F-59655 Villeneuve d'Ascq, France*
[2] *Department of Engineering, University of Ferrara, Via Saragat 1, 44122 Ferrara, Italy*

Compiled December 4, 2019

We investigate the frequency comb spectrum produced in an optical fiber via multiple four-wave mixing pumped in the normal group-velocity region close to the zero-dispersion wavelength. We show that the dynamics is strongly affected by shock formation. In this regime, the resonant radiation emitted by the shock waves correctly explains the enhanced spectral peaks in the comb. The resonant frequencies found by means of perturbation theory accurately fit those observed from the numerical simulation based on the generalised nonlinear Schrödinger equation.

OCIS codes: (060.4370) Nonlinear optics, fibers; (190.5530) Pulse propagation and temporal solitons

Frequency combs generated via multiple four-wave mixing (mFWM) are attracting strong interest. The most extended combs have been produced by exploiting the excitation of an extremely wide set of modes of microcavities via mFWM pumped in the regime of anomalous group-velocity dispersion (GVD) [1]. However, the combs can be produced also in cavity-less configurations, e.g. in a fiber or Kerr photonic wire. Although their extension is not comparable, they offer the possibility to tune the comb repetition through the choice of pump frequencies $\Omega_{\pm 1} = \Omega_0 \pm \Omega/2$ equally detuned central frequency Ω_0. Multiple orders are produced at $\Omega_{\pm m} = \Omega_0 \pm m\Omega/2$, $m = 3, 5, 7, ...$ through cascaded mFWM [2, 3] (note that for strong pump power imbalance, first-order FWM can be viewed essentially as the idler generation, followed by cascaded signal-idler multiple pairs). In both the balanced and the imbalanced cases, the mismatch induced by GVD sets fundamental limitations to the generation efficiency of multiple orders. This can be overcome in fibers by operating sufficiently close to the zero-dispersion wavelength (ZDW), which allows for generating tens of FWM orders [4–8]. Pumping in the normal (modulationally stable [9]) GVD regime appears to be particularly intriguing since strong spectral broadening is intimately linked to the recently demonstrated excitation of dispersive shock waves (DSWs) via wave-breaking in mFWM [8,10]. Temporal DSWs or undular bores, i.e. trains of fast oscillations emitted beyond points of breaking (gradient catastrophies), are indeed responsible, in frequency domain, for enhanced comb broadening.

In this Letter, our aim is to assess the effect of higher-order dispersion on such phenomenon. In particular we show that the DSWs have deep impact on the spectral features of the comb since they are responsible for spectral peaks associated with the growth of dispersive waves at resonant frequencies where phase-matching can be achieved. In this respect, the phenomenon has the same physical origin of soliton radiation [11, 12] (see also [13, 14] and references therein, for recent advances). However, when the radiation is shed by a shock wave (instead of a soliton), a major difference arises from the impact that the velocity of the shock front has on phase matching [15–17]. Here we show that such conclusion holds true for combs due to mFWM as well. We show that, in order to predict the enhanced spectral peaks in the discrete spectrum, one can successfully use the phase-matching formula employed in Ref. [16] for pulses, though we propose a different derivation of the equation based on perturbation theory [18]. Although such formula works at all orders of dispersion, we specifically focus on the effect of third-order dispersion (TOD, also recently considered for cavity combs [19]), discussing in details different possible regimes.

Let us start from the following generalised nonlinear Schrödinger equation (NLSE) written by adopting the so-called semiclassical dimensionless scaling [8, 10, 16]

$$i\varepsilon \frac{\partial u}{\partial z} + d(\partial_t)u + |u|^2 u = 0, \qquad (1)$$
$$d(\partial_t) = \sum \frac{\beta_n}{n!} (i\varepsilon\partial_t)^n = -\frac{\beta_2\varepsilon^2}{2}\partial_t^2 - i\frac{\beta_3\varepsilon^3}{6}\partial_t^3 + \frac{\beta_4\varepsilon^4}{24}\partial_t^4 + \dots$$

where the sum is over $n \geq 2$, and we adopted the same normalization as in Ref. [8], i.e. $|u(z,t)|^2$, z and t stand for the instantaneous power, distance, and retarded time in units of injected power P_t, characteristic length and time $L = \sqrt{L_{nl}L_d}$ and $T_0 = \pi/\Omega$ [$L_{nl} = (\gamma P_t)^{-1}$ and $L_d = T_0^2/\partial_\Omega^2 k$ are nonlinear and dispersion lengths, respectively, γ being the standard fiber nonlinear coefficient). We are interested in the evolution ruled by Eq. (1) subject to the dual-frequency initial condition

$$u_0(t) = \sqrt{\eta}\exp(i\omega_p t/2) + \sqrt{1-\eta}\exp(-i\omega_p t/2), \qquad (2)$$

with fixed normalized frequency $\omega_p \equiv |\Omega_{\pm 1}|T_0 = \pi$, whereas η accounts for the possible imbalance of the input spectral lines. The weakness of dispersion is measured by the key parameter $\varepsilon \equiv \sqrt{L_{nl}/L_d}$, which allows to express the dispersion operator $d(\partial_t)$ in Eq. (1) as an asymptotic power series of ε by introducing the normalized coefficients $\beta_n = \partial_\Omega^n k/\sqrt{(L_{nl})^{n-2}|\partial_\Omega^2 k|^n}$ (we keep the symbol β_2 to highlight the contribution due to GVD, though our normalization implies $|\beta_2| = 1$).

When pumped in the regime of weak normal dispersion ($\beta_2 = 1$), mFWM is characterized by the formation of DSWs [8, 10]. When DSWs are excited sufficiently

close to a ZDW, they are expected to radiate, owing to phase-matching with linear waves induced by higher-order dispersion [15,16]. An example of this resonant radiation (RR) ruled by TOD (we set $\beta_3 = 0.3$) is shown in Fig. 1 for an imbalanced input [$\eta = 0.3$ in Eq. (2)]. The colormap evolution in Fig. 1(a) clearly shows that the initial waveform undergoes wavebreaking around $z \sim 0.4$. The mechanism of breaking has been analyzed in details in Ref. [8,10] and involves two gradient catastrophes occurring across each minimum of the injected modulation envelope. The GVD regularizes the catastrophes leading to the formation of two DSWs, i.e. fast wavetrains that expand inside characteristic shock fans delimited by the deepest oscillation (DSW leading edge) and the most shallow one (DSW trailing edge) in (t, z) plane. The individual oscillations in the trains exhibits dark soliton features, moving with nearly constant darkness and velocity inversely proportional to it. Importantly the breaking scenario is weakly affected by TOD, except for a major difference which is clear from the comparison of the snapshots displayed in Fig. 1(b). In the presence of TOD, one can notice indeed that the darkest soliton-like oscillation emits RR. This radiation has much higher frequency than the comb spacing and turns out to be generated over the CW plateau of the leading edge labeled u_0. This is clear from Fig. 1(c), which shows the enhancement of such frequency at the distance of breaking where the strong spectral broadening associated with the shock acts as a seed for the phase-matched (resonant) frequency. In order to show the origin of the spectral peak shown in Fig. 1(c), we compare in Fig. 1(d) the spectra at $z = 0.7$ in the presence and in the absence of TOD, respectively. In the latter case it is evident that the comb does not exhibit any resonant enhancement of high frequencies.

The frequency of the RR shown in Fig. 1(d) can be predicted by applying a perturbation approach which accounts for dispersion at all orders [13, 18]. We start by assuming a radiating shock front u_s which travels with invariant profile at definite velocity $V = dt/dz$ In other words we consider the local edge of a solution $u(z,t) = u_s(\tau)\exp(ik_s z)$ of Eq. (1) with dispersion truncated at second-order, where $\tau = t - Vz$ and k_s is the nonlinear wavenumber of the shock. We account for perturbations to this front due to higher-order dispersion by assuming a perturbed field of the form $u = [u_s(\tau) + p(z,\tau)]\exp(ik_s z)$. By substituting u in Eq. (1), we obtain, after linearization ($|p| \ll |u_s|$), the following evolution equation for p

$$i\varepsilon\frac{\partial p}{\partial z} + \hat{d}(\partial_\tau)p + 2|u_s|^2 p + u_s^2 p^* = F \qquad (3)$$

where $F = -\left[d(\partial_\tau) - \beta_2(i\epsilon\partial_\tau)^2/2\right] u_s$ is a forcing term with zero wavenumber, and $\hat{d}(\partial_\tau) \equiv d(\partial_\tau) - iV\varepsilon\partial_\tau$. Setting $p(z,\tau) = A(z)\exp[i(kz - \omega\tau)] + B^*(z)\exp[-i(kz - \omega\tau)]$, we find that Eq. (3) for $F = 0$ (i.e. for free-running waves) reduces to the following system for the Stokes-antiStokes amplitudes $a(z) = [A(z)\ B(z)]^T$

$$i\varepsilon\frac{da}{dz} + Ca = 0, \qquad (4)$$

$$C = \begin{pmatrix} D(\omega) - \varepsilon k & u_s^2 \\ -(u_s^*)^2 & -D(-\omega) - \varepsilon k \end{pmatrix}, \qquad (5)$$

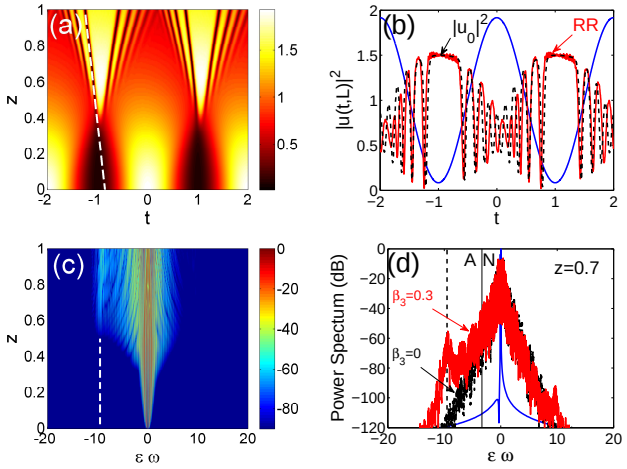

Fig. 1. RR emitted by shock with asymmetric pumping $\eta = 0.3$, and $\varepsilon = 0.04$: (a) temporal and (c) spectral colormap evolution for $\beta_3 = 0.3$; (b) temporal snapshots ($\beta_3 = 0$ dashed; $\beta_3 = 0.3$, solid); (d) Comparison between spectral output with/without β_3 (blue solid line is the input). Dashed line in (a) highlights the DSW edge velocity $V = -0.4$. Vertical dashed line in (c,d) indicates ω_{RR} from Eq. (8). A/N in (d) stands for anomalous/normal GVD domains.

where $D(\omega) = \tilde{d}(\varepsilon\omega) + 2|u_s|^2 - \varepsilon k_s$, and $\tilde{d}(\varepsilon\omega) = \sum \frac{\beta_n}{n!}(\varepsilon\omega)^n - (\varepsilon\omega)V$ is the Fourier transform of $\hat{d}(\partial_t)$. The dispersion relation $\kappa = \kappa(\varepsilon\omega)$ of such waves is found by imposing $det(C) = 0$, which yields the following two branches $\kappa = \kappa_\pm(\varepsilon\omega)$

$$\varepsilon\kappa_\pm = \frac{d_{odd}}{2} \pm \frac{1}{2}\sqrt{d_{even}[d_{even} + 4|u_0|^2]}, \qquad (6)$$

where $d_{odd} \equiv \tilde{d}(\varepsilon\omega) - \tilde{d}(-\varepsilon\omega)$ and $d_{even} \equiv \tilde{d}(\varepsilon\omega) + \tilde{d}(-\varepsilon\omega)$, and we have considered that $k_s = |u_0|^2$ is the Kerr wavenumber shift over the CW plateau (upper state of the shock front) with power $|u_0|^2$ where RR is emitted [see Fig. 1(b)]. Frequencies $\omega = \omega_{RR}$ such that $\kappa_\pm = \kappa(\varepsilon\omega_{RR}) = 0$ can grow because they become resonant with the forcing F in Eq. (3). They arise in pairs ($\omega = \pm|\omega_{RR}|$) due to symmetry of the problem. Note, however, that the wave amplitude that grows at such frequencies is generally very different [see Fig. 1(d)], being related to the eigenvectors of the matrix.

A sufficiently accurate estimate for ω_{RR} can be obtained by expanding the square root in Eq. (6) under the hypothesis $|u_0|^2 \ll |d_{even}|$, which yields

$$\tilde{d}(\pm\varepsilon\omega_{RR}) + |u_0|^2 = 0. \qquad (7)$$

While this approach permits to treat dispersion at all orders, we continue to analyze the effect of the usually dominant term, i.e. TOD ($\beta_3 \neq 0$, $\beta_n = 0$, $n \geq 4$). In this case Eq. (7) explicitly reads as (we consider the upper sign in Eq. (7), the other case can be derived with obvious symmetry arguments)

$$\left[\beta_3\frac{(\varepsilon\omega_{RR})^3}{6} + \beta_2\frac{(\varepsilon\omega_{RR})^2}{2} - V(\varepsilon\omega_{RR})\right] + |u_0|^2 = 0. \qquad (8)$$

Equation (8) coincides with the condition derived in Ref. [16] on simple physical ground. The square bracket represents the wavenumber of linear waves while the remaining term stands for the nonlinear correction induced through cross-phase modulation from the u_0 plateau over which radiation is emitted [see Fig. 1(b)].

In the limit $V = 0$, also neglecting the nonlinear correction $|u_0|^2$, Eq. (8) gives the approximated result $\varepsilon\omega_{RR} = -3\beta_2/\beta_3$, or $\Omega_{RR} = \omega_{RR}/T_0 = -3\partial^2_\Omega k/\partial^3_\Omega k$ in physical units. This is equivalent to the original result derived for bright soliton [11, 12] and shown to correspond to phase-matching of a cascaded mixing process in Ref. [6]. For mFWM the latter estimate can be considered accurate enough when the nonlinear effects do not dominate over dispersive ones ($\varepsilon \sim 1$), or in other words when relatively few FWM orders are generated. Viceversa in the weakly dispersive regime ($\varepsilon \ll 1$) which involves wave-breaking and efficient generation of extended combs, one needs to resort to Eq. (7) in order to account for the spectral features observed in the numerics. A comparison between the two regimes is carried out in Fig. 2 for symmetric pumping [$\eta = 0.5$ in Eq. (2)]. Figure 2(a-b) are obtained in the moderately nonlinear regime with $\varepsilon = 0.4$. In this case the modulation propagates without exhibiting any breaking phenomenon. In frequency domain, the mFWM orders decay monotonically towards high frequencies, while crossing the ZDW over the low frequency side, the $m = -5$ order turns out to be resonantly enhanced. The frequency of this line is well described by the approximation $\varepsilon\omega_{RR} = -3\beta_2/\beta_3$ [vertical dash-dotted line in Fig. 2(b)]. Viceversa in the strongly nonlinear regime ($\varepsilon = 0.04$) the wavebreaking qualitatively alters the previous scenario, as shown in Fig. 2(c-d). In the case $\beta_3 = 0$, the symmetric pump is a degenerate case [8, 10], where the two points of breaking coalesce in time over the modulation minima and a black soliton-like pulse (with $V = 0$) emerge, separating two perfectly symmetric DSW [see also Fig. 4(c)]. The presence of TOD breaks the symmetry in time and induces the central filament to acquire a non-zero velocity ($V \sim 0.05$). The latter is small enough for the approximation $\varepsilon\omega_{RR} = -3\beta_2/\beta_3$ to retain its validity. However the spectrum shown in Fig. 2(d) exhibits also an additional peak of the comparable amplitude which is resonantly enhanced by the front of the DSW traveling with velocity $V = -0.59$ [see Fig. 2(c), where two radiating edges (solitons) are highlighted by dashed lines, whose slopes fix V].

When a considerable imbalance is introduced in the initial beat, the DSW leading edges which are responsible for the RR travel at higher absolute velocities V as shown in Fig. 3(a) for $\eta = 0.8$. The RR peaks are due indeed to solitons traveling with opposite velocities [highlighted in Fig. 3(a)] and comparable darkness [see snapshots in Fig. 3(b)]. In this case, the RR become stronger since the resonant frequencies move at lower frequencies [Fig. 3(c,d)]. In order to correctly predict both peaks one must employ Eq. (8), while the approximation $\varepsilon\omega_{RR} = -3\beta_2/\beta_3$ introduces a considerable error.

Finally we point out that so far we have considered a perturbative role of TOD ($|\beta_3| < 0.5$). Larger perturbations in the generalized NLSE can qualitatively alter the shock dynamics [20]. This turns out to be the case also

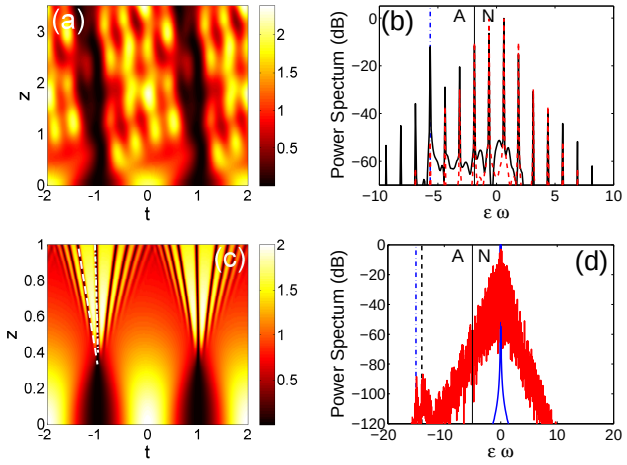

Fig. 2. Comparison of mFWM spectra in the non-shock (a-b) and shock (c-d) regime for symmetric pumping $\eta = 0.5$. Parameters: (a-b) $\beta_3 = 0.53$, $\varepsilon = 0.4$; (c-d) $\beta_3 = 0.2$, $\varepsilon = 0.04$. The blue dash-dotted line stands for the approximation $\varepsilon\omega_{RR} = -3\beta_2/\beta_3$ [6] valid for $V \simeq 0$. The other RR peak (black dashed line) is given by Eq. (8) with $V = -0.59$.

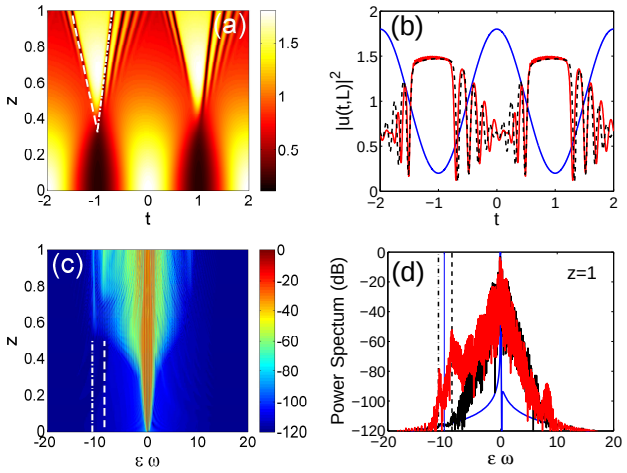

Fig. 3. RR emitted by shock with asymmetric pumping $\eta = 0.8$ (a) temporal and (c) spectral colormap evolution for $\beta_3 = 0.3$; (b) temporal snapshots ($\beta_3 = 0$ and $\beta_3 = 0.3$); (d) spectral output with/without β_3. Dashed lines in (a) highlight shock velocities $V = -0.77$ and $V = 0.435$. Vertical dashed and dash-dotted lines in (d) indicates ω_{RR} calculated from Eq. (8), whereas solid line stands for $\varepsilon\omega_{RR} = -3\beta_2/\beta_3$ [6]. Here $\varepsilon = 0.04$.

for mFWM under stronger TOD, as illustrated in Fig. 4, which report novel regimes bearing no similarity with the case of the GVD-dominated dispersion.

First, we show that a higher TOD allows for the formation of radiating classical shock waves, i.e. a disturbance which propagates as a non-oscillatory jump. Indeed, in the presence of two shock fans, the effect of TOD is to open up one of the fan and to induce narrowing of the other one, until the latter eventually reduces to a pure

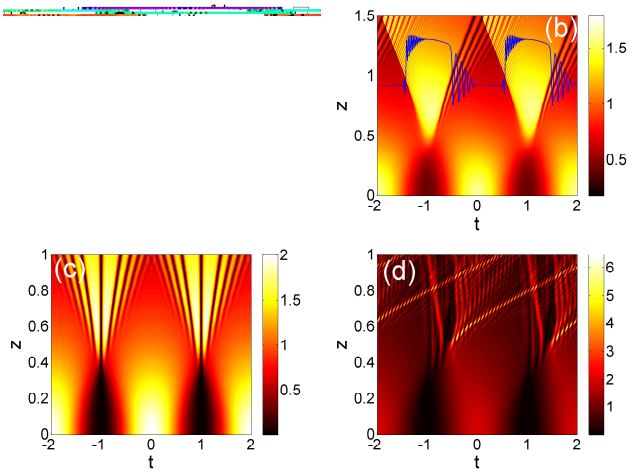

Fig. 4. Non perturbative regimes: (a-c) Temporal colormap for $\beta_3 = 0$ and (b-d) $\beta_3 \neq 0$. (b) RR from a quasi-classical shock wave, with $\beta_3 = 0.6$. Here $\eta = 0.1$, $\varepsilon = 0.02$. Snapshot at $z = 1$ superimposed. (d) Mixed-type catastrophe for $\beta_3 = 1.5$. Here $\eta = 0.5$, $\varepsilon = 0.04$.

front for sufficiently large β_3. This situation is illustrated in Fig. 4(a,b), where we contrast the DSW temporal pattern generated in the absence of TOD with the one generated for $\beta_3 = 0.6$. The fan of the DSW which is propagating leftwards in Fig. 4(a) shrinks completely for $\beta_3 = 0.6$ [see Fig. 4(b)], leaving a jump which propagates nearly unchanged. This front is still efficiently radiating at a resonant frequency well described by Eq. (8) with a velocity V which is entirely determined by the jumps in intensity and chirp (this follows from so-called Rankine-Hugoniot condition for classical shock waves, whose discussion is beyond the scope of this paper. We refer the reader to Ref. [16] for a detailed discussion of this point). Such a velocity remains nearly unaffected by the collisions with the DSW arising from the neighbor period.

Second, when TOD is even larger ($|\beta_3| > 1$), it can deeply alter the breaking scenario, as shown in Fig. 4(c,d) for symmetric pumping ($\eta = 0.5$). For $\beta_3 = 0$ breaking occurs at $z \sim 0.4$ and gives rise to two symmetric DSWs separated by a central filament as shown in Fig. 4(c). For $\beta_3 = 1.5$ [see Fig. 4(d)] the primary breaking, still occurring at $z \sim 0.4$, is followed by a secondary catastrophe at $z \sim 0.5, t \sim 1 \pm 0.5$, beyond which the system exhibits the emission of localized breather-like excitations with large velocity. The secondary breaking is reminiscent of that occurring for the focusing semi-classical NLS [21] (since locally the eigenvelocities of the hydrodynamic limit become complex conjugate as outlined in Ref. [16]). This allows us to conclude that the system exhibits, for $|\beta_3| \sim 1$, a coexistence of locally different wavebreaking mechanisms that are characteristic of both the defocusing and focusing NLSE.

Finally, we emphasize that the shock-induced resonances (as in Figs. 1-3) should be readily seen experimentally by exploiting the set-up of Ref. [8], where at the largest power of 37 dBm, one obtains $\varepsilon \simeq 0.04$ and $L_{nl} \simeq 115$ m. In this regime $\beta_3 = 0.3$ corresponds to a realistic physical TOD $\partial^3_\Omega k = \beta_3 \sqrt{L_{nl} |\partial^2_\Omega k|^3} = 0.6$ ps^3/km ($\partial^2_\Omega k = 3.2$ ps^2/km).

In summary, we have predicted that mFWM broadband combs produced in the regime of wave-breaking exhibit one or more marked spectral peaks that are due to the resonant radiation shed by DSWs. The resonant frequencies observed in the numerics can be accurately predicted on the basis of phase-matching arguments that involve the determination of the shock edge velocity.

The authors acknowledge discussions with J. Fatome and G. Millot, as well as funding by the Italian Ministry of University and Research (MIUR), under grant PRIN 2012BFNWZ2 and by the Agence Nationale de la Recherche through the ANR TOPWAVE project.

References

1. P. Del'Haye, A. Schliesser, O. Arcizet, T. Wilken, R. Holzwarth, and T. J. Kippenberg, Nature **450**, 1214 (2007).
2. J. R. Thompson and R. Roy, Phys. Rev. A **43**, 4987 (1991).
3. S. Trillo, S. Wabnitz, and T.A.B. Kennedy, Phys. Rev. A **50**, 1732 (1994).
4. S. Jr. Cerqueira Arismar, J. M. Chavez Boggio, A. A. Rieznik, H. E. Hernandez-Figueroa, H. L. Fragnito, and J. C. Knight, Opt. Express **16**, 2816 (2008).
5. F. C. Cruz, Opt. Express **16**, 16237 (2008).
6. M. Erkintalo, Y. Q. Xu, S. G. Murdoch, J. M. Dudley, and G. Genty, Phys. Rev. Lett. **109**, 223904 (2012).
7. Y. H. Li, Y. Y. Zhao, and L. J. Wang, Opt. Lett. **37**, 3441 (2012).
8. J. Fatome, C. Finot, G. Millot, A. Armaroli, and S. Trillo, Phys. Rev. X **4**, 021022 (2014).
9. J. Fatome, C. Finot, A. Armaroli, and S. Trillo, Opt. Lett. **38**, 181 (2013).
10. S. Trillo and A. Valiani, Opt. Lett. **35**, 3967 (2010).
11. P. K. A. Wai, C. R. Menyuk, H. H. Chen, and Y. C. Lee, Opt. Lett. **12**, 628 (1987).
12. N. Akhmediev and M. Karlsson, Phys. Rev. A **51**, 2602 (1995).
13. D. V. Skryabin and A. V. Gorbach, Rev. Mod. Phys. **82**, 1287 (2010).
14. P. Colman, S. Combrié, G. Lehoucq, A. de Rossi, and S. Trillo, Phys. Rev. Lett. **109**, 093901 (2012).
15. M. Conforti and S. Trillo, Opt. Lett. **38**, 3815 (2013).
16. M. Conforti, F. Baronio, and S. Trillo, Phys. Rev. A **89**, 013807 (2014).
17. K. E. Webb, Y. Q. Xu, M. Erkintalo, and S. G. Murdoch, Opt. Lett. **38**, 151 (2013).
18. D. V. Skryabin and A. V. Yulin, Phys. Rev. E **72**, 016619 (2005).
19. P. Padras-Rivas, D. Gomila, F. Leo, S. Coen, and L. Gelens, Opt. Lett. **39**, 2971 (2014).
20. M. Crosta, A. Fratalocchi, S. Trillo, Phys. Rev. A **85**, 043607 (2012).
21. P. D. Miller and S. Kamvissis, Phys. Lett. A **247**, 75 (1998).

Informational Fifth Page

References

1. P. Del'Haye, A. Schliesser, O. Arcizet, T. Wilken, R. Holzwarth, and T. J. Kippenberg, "Optical frequency comb generation from a monolithic microresonator", Nature **450**, 1214 (2007).
2. J. R. Thompson and R. Roy, "Nonlinear dynamics of multiple four-wave mixing processes in a single-mode fiber," Phys. Rev. A **43**, 4987 (1991).
3. S. Trillo, S. Wabnitz, and T.A.B. Kennedy, "Nonlinear dynamics of dual-frequency pumped multiwave mixing in optical fibers", Phys. Rev. A **50**, 1732 (1994).
4. S. Jr. Cerqueira Arismar, J. M. Chavez Boggio, A. A. Rieznik, H. E. Hernandez-Figueroa, H. L. Fragnito, and J. C. Knight, "Highly efficient generation of broadband cascaded four-wave mixing products, Opt. Express **16**, 2816 (2008).
5. F. C. Cruz, "Optical frequency combs generated by four-wave mixing in optical fibers for astrophysical spectrometer calibration and metrology", Opt. Express **16**, 16237 (2008).
6. M. Erkintalo, Y. Q. Xu, S. G. Murdoch, J. M. Dudley, and G. Genty, "Cascaded Phase Matching and Nonlinear Symmetry Breaking in Fiber Frequency Combs", Phys. Rev. Lett. **109**, 223904 (2012).
7. Y. H. Li, Y. Y. Zhao, and L. J. Wang, "Demonstration of almost octave-spanning cascaded four-wave mixing in optical microfibers", Opt. Lett. **37**, 3441 (2012).
8. J. Fatome, C. Finot, G. Millot, A. Armaroli, and S. Trillo, "Observation of optical undular bores in multiple four-wave mixing", Phys. Rev. X **4**, 021022 (2014).
9. J. Fatome, C. Finot, A. Armaroli, and S. Trillo, "Observation of modulationally unstable multi-wave mixing", Opt. Lett. **38**, 181 (2013).
10. S. Trillo and A. Valiani, "Hydrodynamic instability of four-wave-mixing", Opt. Lett. **35**, 3967 (2010).
11. P. K. A. Wai, C. R. Menyuk, H. H. Chen, and Y. C. Lee, "Soliton at the zero-group-dispersion wavelength of a single-model fiber", Opt. Lett. **12**, 628 (1987).
12. N. Akhmediev and M. Karlsson, " Cherenkov radiation emitted by solitons in optical fibers", Phys. Rev. A **51**, 2602 (1995).
13. D. V. Skryabin and A. V. Gorbach, "Looking at a soliton through the prism of optical supercontinuum", Rev. Mod. Phys. **82**, 1287 (2010).
14. P. Colman, S. Combrié, G. Lehoucq, A. de Rossi, and S. Trillo, "Blue Self-Frequency Shift of Slow Solitons and Radiation Locking in a Line-Defect Waveguide", Phys. Rev. Lett. **109**, 093901 (2012).
15. M. Conforti and S. Trillo, "Dispersive wave emission from wave breaking", Opt. Lett. **38**, 3815 (2013).
16. M. Conforti, F. Baronio, and S. Trillo, "Resonant radiation shed by dispersive shock waves", Phys. Rev. A **89**, 013807 (2014).
17. K. E. Webb, Y. Q. Xu, M. Erkintalo, and S. G. Murdoch, "Generalized dispersive wave emission in nonlinear fiber optics", Opt. Lett. **38**, 151 (2013).
18. D. V. Skryabin and A. V. Yulin, "Theory of generation of new frequencies by mixing of solitons and dispersive waves in optical fibers", Phys. Rev. E **72**, 016619 (2005).
19. P. Padras-Rivas, D. Gomila, F. Leo, S. Coen, and L. Gelens, "Third-order chromatic dispersion stabilizes Kerr frequency combs", Opt. Lett. **39**, 2971 (2014).
20. M. Crosta, A. Fratalocchi, S. Trillo, "Crossover dynamics of dispersive shocks in Bose-Einstein condensates characterized by two and three-body interactions", Phys. Rev. A **85**, 043607 (2012).
21. P. D. Miller and S. Kamvissis, "On the semiclassical limit of the focusing NLSE", Phys. Lett. A **247**, 75 (1998).